

ON THE POST-KEPLERIAN CORRECTIONS TO THE ORBITAL PERIODS OF A TWO-BODY SYSTEM AND THEIR APPLICATION TO THE GALACTIC CENTER

LORENZO IORIO¹, FUPENG ZHANG²

¹Ministero dell’Istruzione, dell’Università e della Ricerca (M.I.U.R.)-Istruzione
 Permanent address for correspondence: Viale Unità di Italia 68, 70125, Bari (BA), Italy; lorenzo.iorio@libero.it and

²School of Physics and Astronomy, Sun Yat-Sen University, Guangzhou 510275, China; zhangfp7@mail.sysu.edu.cn

Draft version October 19, 2018

ABSTRACT

Detailed numerical analyses of the orbital motion of a test particle around a spinning primary are performed. They aim to investigate the possibility of using the post-Keplerian (pK) corrections to the orbiter’s periods (draconitic, anomalistic and sidereal) as a further opportunity to perform new tests of post-Newtonian (pN) gravity. As a specific scenario, the S-stars orbiting the Massive Black Hole (MBH) supposedly lurking in Sgr A* at the center of the Galaxy is adopted. We, first, study the effects of the pK Schwarzschild, Lense-Thirring and quadrupole moment accelerations experienced by a target star for various possible initial orbital configurations. It turns out that the results of the numerical simulations are consistent with the analytical ones in the small eccentricity approximation for which almost all the latter ones were derived. For highly elliptical orbits, the size of all the three pK corrections considered turn out to increase remarkably. The periods of the observed S2 and S0-102 stars as functions of the MBH’s spin axis orientation are considered as well. The pK accelerations considered lead to corrections of the orbital periods of the order of 1 – 100 d (Schwarzschild), 0.1 – 10 h (Lense-Thirring) and 1 – 10³ s (quadrupole) for a target star with $a = 300 - 800$ AU and $e \approx 0.8$, which could be possibly measurable by the future facilities.

Keywords: Galaxy: center – gravitation – relativistic processes – stars: kinematics and dynamics – time

1. INTRODUCTION

The periodic evolutions of the orbits of a binary system can be described differently by some characteristic orbital time spans that pertain the crossing of different locations in the sky: the draconitic, anomalistic and sidereal orbital periods, which are measured according to two consecutive crossings of the lines of the nodes, periapsis, and a given reference direction in the sky plane, respectively (Capderou 2005). In the purely Keplerian case, all of them coincide, while the degeneration is removed when additional accelerations with respect to the Newtonian monopole are present in the equations of motion. Thus, measuring them would, in principle, provide a further way to test post-Newtonian (pN) gravity in several independent scenarios. Recently, the post-Keplerian (pK) corrections to the two-body sidereal, draconitic and anomalistic orbital periods induced by some pK Newtonian and pN accelerations were analytically calculated in a perturbative framework (Iorio 2016). These pK corrections of the orbital periods are potentially measurable in some astronomical and astrophysical environments like Earth’s satellites (e.g., Kassimeno 1966; Mashhoon et al. 2001), Solar and exoplanetary systems (Iorio 2016).

The stellar system made of the so-called “S-stars” which orbit the Massive Black Hole (MBH) in the Galactic Center (GC) provide an unique test-bed for probing general relativity (GR) in the strong gravity regime. Since 1992, the S-stars in the GC have been detected and traced by the Very Large Telescope (VLT) (Gillessen et al. 2009), New Technology Telescope (NTT) and Keck telescope (Ghez et al. 2008). These observations have provided so far accurate constraints on the mass and distance of the Galactic MBH. In the near future, the GRAVITY facility (Gillessen et al. 2010) on the Very Large Telescope Interferometer (VLTI), the Thirty Meter Telescope (TMT) (Skidmore et al. 2015), and the European Extremely Large Telescope (E-ELT) (Vernin et al. 2011), which are ex-

pected to perform extremely accurate measurements of the stars’ position and redshift, can be able to reveal the GR effects hidden in their tracked motion (e.g., Zhang et al. 2015; Angéilil et al. 2010; Angéilil & Saha 2010, 2011; Merritt et al. 2010; Iorio 2011a,b; Yu et al. 2016). In the meantime, the pK corrections of the aforementioned periods could be measurable if the evolutions of the orbital elements can be inferred from these observables.

Here, we numerically investigate the pK corrections of S-stars’ orbital periods under various initial conditions and discuss their possible applications for GR tests. The paper is organized as follows. In Section 2, we briefly describe the adopted pN accelerations and the numerical strategies in obtaining the different orbital periods. Section 3 collects the results obtained for the Schwarzschild-like, Lense-Thirring and the quadrupole momentum effects. Section 4 provides a discussion of the results obtained, which are finally summarized in Section 5.

2. THE NUMERICAL METHOD USED

In our numerical simulations, we integrate the equations of motion of a test star moving around a central black hole under the action of the Newtonian and pN accelerations. The standard Newtonian monopole is given by $a_N = -GM/r^2$, where M is the mass of the central black hole, G is the gravitational constant, and r is the distance of the test particle from M . In this work, we also consider the effects of following pK accelerations (Soffel 1989; Brumberg 1991) of both Newtonian and pN origin:

- The pN Schwarzschild-type gravitoelectric (GE) acceleration due to the static mass:

$$\mathbf{a}_{\text{GE}} = -\frac{GM}{r^3 c^2} \left[\left(v^2 - 4 \frac{GM}{r} \right) \mathbf{r} - 4(\mathbf{r} \cdot \mathbf{v}) \mathbf{v} \right], \quad (1)$$

which is the largest 1pN term in the pN formalism. Here, c is the speed of light, \mathbf{r} and \mathbf{v} are the position and velocity vectors of the star, respectively, while $v = |\mathbf{v}|$ is its speed.

- The pN Lense-Thirring gravitomagnetic acceleration due to the slow rotation of the central body:

$$\mathbf{a}_{\text{LT}} = \frac{2GS}{c^2 r^3} \left[3(\hat{\mathbf{S}} \cdot \hat{\mathbf{r}})\hat{\mathbf{r}} \times \mathbf{v} + \mathbf{v} \times \hat{\mathbf{S}} \right], \quad (2)$$

where $\hat{\mathbf{r}}$ is the versor of the position vector. In the BH case, the angular momentum is given by $S = \chi M^2 G c^{-1}$, where χ is the dimensionless spin parameter, while $\hat{\mathbf{S}}$ is the unit vector of the spin.

- The Newtonian acceleration due to the quadrupole mass moment J_2 of the primary:

$$\mathbf{a}_{J_2} = \frac{J_2 G M R_e^2}{2r^4} \left\{ \left[5(\hat{\mathbf{S}} \cdot \hat{\mathbf{r}})^2 - 1 \right] \hat{\mathbf{r}} - 2(\hat{\mathbf{S}} \cdot \hat{\mathbf{r}})\hat{\mathbf{S}} \right\}. \quad (3)$$

For a rotating BH, an acceleration analogue to Equation 3 arises in a general relativistic context in such a way that $J_2 G M R_e^2 \rightarrow Q = -\chi^2 G^3 M^3 c^{-4} = -S^2 G c^{-1} M^{-1}$ (Geroch 1970; Hansen 1974), and $q = -\chi^2$ is the dimensionless quadrupole moment.

The six orbital elements a (orbital semimajor axis), e (eccentricity), I (Inclination to the reference $\{x, y\}$ plane which coincides with the plane of the sky as in Fig. 1 of (Zhang et al. 2015)), Ω (longitude of the ascending node), ω (argument of the periapsis), f (true anomaly) of the target star are calculated according to the state vector of the star: x, y, z and $\dot{x}, \dot{y}, \dot{z}$ at any instant. Then, the different periods can be obtained as follows: (1) The draconitic period is the time interval between $u = 0$ and $u = 2\pi$; here, $u = \omega + f$ is the argument of latitude. (2) The anomalistic is the time interval between $f = 0$ and $f = 2\pi$. (3) The sidereal period is the time interval between $l = 0$ and $l = 2\pi$, where $l = \Omega + \omega + f$ is the true longitude¹. We denote P_{dra} , P_{ano} and P_{sid} as the draconitic, anomalistic and sidereal periods, respectively.

Each effect of the Schwarzschild, Lense-Thirring or quadrupole moment can be calculated by switching the corresponding accelerations showed in Equation 1-3 on and off and, then, inspect the difference of these periods. The perturbed period by these effects are denoted as $\delta_{\text{GE}}P$, $\delta_{\text{LT}}P$ and $\delta_Q P$, respectively. Here, P could be any of P_{dra} , P_{ano} or P_{sid} .

We adopt the code DORPRI5 based on the explicit fifth (fourth)-order Runge Kutta method (Dormand & Prince 1980; Hairer, Norsett & Wanner 1987) to integrate the equations of motion to obtain the orbital path of the star. The relative integration error is $\leq 10^{-12}$ for all the simulations performed in this work, which is sufficient for the convergence of the numerical results in this study.

Note that, in some cases, the orbit of the target star is initially bound in Newtonian gravity but turns out to be unbound while the pK corrections are considered, especially for those stars with high initial orbital eccentricities. We avoid these unbound orbits as they do not have periodic patterns. In the numerical simulations, we remove the stars that initially have positive specific orbital energy, i.e., $E_{\text{orb}} > 0$. Here E_{orb} is

¹ We notice that the results are the same if the intervals are measured between $u = u_0$ and $u = u_0 + 2\pi$ for arbitrary u_0 , similarly for f and l .

given by (Kidder 1995)

$$E_{\text{orb}} = \frac{1}{2}v^2 - \frac{GM}{r} + \frac{3v^4}{8c^2} + \frac{3v^2}{2c^2} \frac{GM}{r} + \frac{G^2 M^2}{2c^2 r^2}. \quad (4)$$

3. RESULTS

First, for each of the pK effects considered, we calculate the time series of the element $u(t)$, $f(t)$, $l(t)$, with and without the pK accelerations by adopting the same initial conditions for the target star in both the integrations. Then, for each run, we estimate the periods P according to the resulting numerically integrated time series of $u(t)$, $f(t)$, $l(t)$. Finally, we get the difference δP of such periods between each couple of runs, which shows the effects of the corresponding pK acceleration.

In the following, we will assume that the mass of the central MBH is $M_{\bullet} = 4 \times 10^6 M_{\odot}$, which approximates the one found in the Galactic center (e.g., Gillessen et al. 2009; Ghez et al. 2008). As far as the orbital geometries of the test particle adopted are concerned, we will consider both fictitious orbital configurations and those of the so-far discovered S2 ($a_0 = 984$ AU, $e_0 = 0.88$, $I_0 = 135^\circ$, $\Omega_0 = 225^\circ$, $\omega_0 = 243^\circ$) and S0-102 ($a_0 = 848$ AU, $e_0 = 0.68$, $I_0 = 151^\circ$, $\Omega_0 = 175^\circ$, $\omega_0 = 5^\circ$). Since the gravitoelectric anomalistic correction (cfr. Equation (72) of Iorio (2016)) and all the three corrections due to the quadrupole mass moment (cfr. Equations (65) to (67) of Iorio (2016)) depend on f_0 , we adopted in our simulations the values $f_0 = 157^\circ$ (S2) and $f_0 = 225^\circ$ (S0-102), which correspond to the initial orbital position of S2 and S0-102 in the year 2020, respectively.

The spin axis of the MBH are parameterized by the angle i and ϵ as

$$\hat{S}_x = \sin i \cos \epsilon, \quad (5)$$

$$\hat{S}_y = \sin i \sin \epsilon, \quad (6)$$

$$\hat{S}_z = \cos i, \quad (7)$$

with $0 \leq i \leq \pi$, $0 \leq \epsilon \leq 2\pi$ by considering the angles i , ϵ as free parameters. Here, i is the angle of the spin with respect to the line of sight, and ϵ is the angle between the projected direction of the spin in the plane of the sky and the reference x -axis.

Currently, the spin of the MBH in the GC remains largely unconstrained. The radio observations of Sgr A* provide a weak constraint of the spin parameters of the MBH (Broderick et al. 2009), with 1σ estimated values given by $\chi < 0.4$, $i = 50^{+10}_{-10}^\circ$ and $\epsilon = -20^{+31}_{-16}^\circ$. It is also speculated that the spin axis of the MBH could possibly coincide with the orientation axis of the young stellar disk in the GC, if the latter is the remnant of a previously existing accretion disc (Yu et al. 2016). In this case, the possible spin orientations are $i = 130^\circ$, $\epsilon = 6^\circ$ or $i = 50^\circ$, $\epsilon = 186^\circ$. In this work, we consider both general orientations of the spin axis and the three aforementioned values.

3.1. The 1pN gravitoelectric Schwarzschild-like effect due to a non-rotating primary

The first order theoretical predictions of the 1pN corrections to the orbital period are given by (cfr. Equations 69-72

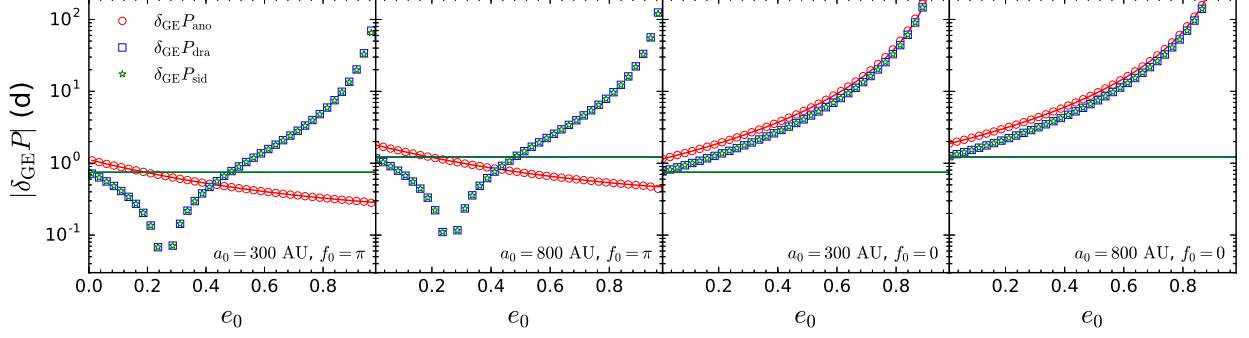


Figure 1. Perturbed orbital periods, in d, due to the 1pN static Schwarzschild-type gravitoelectric field of the MBH. The red open circle, blue square and green star symbols show the simulation’s results for the perturbed anomalistic $\delta_{\text{GE}}P_{\text{ano}}$, draconitic $\delta_{\text{GE}}P_{\text{dra}}$, and sidereal $\delta_{\text{GE}}P_{\text{sid}}$ periods, respectively. Different panels show when a_0 and f_0 take different values (See the legend in the bottom right of each panel). The red, blue and green solid lines show the values theoretically predicted by Equations 8. The blue and green lines, which hold to zero order in the eccentricity, overlap with each other as they have the same value.

of Iorio (2016))

$$\begin{aligned} \delta_{\text{GE}}P_{\text{dra}} &= \frac{12\pi\sqrt{\mu a}}{c^2} + \mathcal{O}(e^n), \quad n \geq 1, \\ \delta_{\text{GE}}P_{\text{ano}} &= \frac{3\pi\sqrt{\mu a}}{c^2(1-e^2)^2} \mathcal{T}_{\text{ano}}^{(\text{GE})}, \\ \delta_{\text{GE}}P_{\text{sid}} &= \frac{12\pi\sqrt{\mu a}}{c^2} + \mathcal{O}(e^n), \quad n \geq 1. \end{aligned} \quad (8)$$

Here,

$$\mathcal{T}_{\text{ano}}^{(\text{GE})} = 6 + 7e^2 + 2e^4 + 2e(7 + 3e^2) \cos f_0 + 5e^2 \cos 2f_0, \quad (9)$$

and $\mu = GM$. Note that such an effect increases as a function of the distance of the star to the MBH ($\propto \sqrt{a}$). Only analytical expressions for $e = 0$ are derived for $\delta_{\text{GE}}P_{\text{dra}}$, $\delta_{\text{GE}}P_{\text{sid}}$ and $\delta_{\text{GE}}P_{\text{ano}}$ while $\delta_{\text{GE}}P_{\text{ano}}$ is obtained explicitly for arbitrary eccentricities.

To explore corrections to the periods induced by the gravitoelectric, Schwarzschild-type acceleration for target stars with various initial conditions, we perform the numerical simulations for an exemplified fictitious target star with the following initial conditions: $a_0 = 300$ AU or 800 AU, $f_0 = 0$ or $f_0 = \pi$, $I_0 = \pi/4$, $\Omega_0 = 0$, $\omega_0 = \pi$, while the eccentricity e_0 is allowed to continuously vary from 0.01 to 0.95. Figure 1 depicts the results of $\delta_{\text{GE}}P_{\text{dra}}(e_0)$, $\delta_{\text{GE}}P_{\text{ano}}(e_0)$, $\delta_{\text{GE}}P_{\text{sid}}(e_0)$ as functions of e_0 . It can be noted that the agreement with the theoretical predictions of Iorio (2016) is remarkable, especially in the case of the anomalistic period for which an exact analytical expression with respect to the eccentricity is available. As far as the draconitic and the sidereal periods are concerned, Equation 8 yield identical predictions for both, valid to zero order in the eccentricity. Our numerically integrated results agree with them in the limit of small values of e_0 . As we can see from Figure 1, the period corrections can vary by 1 ~ 2 orders of magnitude for different values of e_0 if $e_0 \lesssim 0.95$.

According to Equation 8, which is also confirmed by numerical simulations, the anomalistic corrections do not depend on the orbital orientation determined by I , Ω , ω . For the draconitic and sidereal corrections $\delta_{\text{GE}}P_{\text{dra}}$, $\delta_{\text{GE}}P_{\text{sid}}$, however, we found that they depend largely on these parameters. Note that in Figure 1 the draconitic corrections are equal to that of the sidereal ones, i.e., $\delta_{\text{GE}}P_{\text{dra}} = \delta_{\text{GE}}P_{\text{sid}}$; it is a coincidence as we initially set $\Omega_0 = 0$. We find that $\delta_{\text{GE}}P_{\text{dra}} \neq \delta_{\text{GE}}P_{\text{sid}}$ if $\Omega_0 \neq 0$. By performing a large number of numerical simulations, we find that the pK effects of all

the three-types of periods can vary by ~ 1 orders of magnitude if we select arbitrary values of I_0 , Ω_0 , ω_0 , f_0 .

For the currently detected S-star S2 and S0-102, we can obtain their explicit values of the three-types of period corrections. For S2, we have

$$\delta_{\text{GE}}P_{\text{ano}} = 1.4 \text{ d}, \quad (10)$$

$$\delta_{\text{GE}}P_{\text{dra}} = 0.51 \text{ d}, \quad (11)$$

$$\delta_{\text{GE}}P_{\text{sid}} = 0.78 \text{ d}. \quad (12)$$

while for S0-102 our results are

$$\delta_{\text{GE}}P_{\text{ano}} = 1.7 \text{ d}, \quad (13)$$

$$\delta_{\text{GE}}P_{\text{dra}} = 1.6 \text{ d}, \quad (14)$$

$$\delta_{\text{GE}}P_{\text{sid}} = -2.8 \text{ d}. \quad (15)$$

Remarkably, Equation 10 and Equation 13 agree with the corresponding values calculated analytically with Equation 8.

3.2. The 1pN gravitomagnetic Lense-Thirring effect due to the angular momentum of the primary

The theoretical predictions of the 1pN gravitomagnetic corrections to the orbital period are given by (cfr. Equations 74-78 of Iorio (2016))

$$\begin{aligned} \delta_{\text{LT}}P_{\text{dra}} &= \frac{4\pi S}{c^2 M} \left[2(\hat{\mathbf{S}} \cdot \hat{\mathbf{h}}) + (\hat{\mathbf{S}} \cdot \hat{\mathbf{m}}) \cot I \right] + \mathcal{O}(e^n), \quad n \geq 1, \\ \delta_{\text{LT}}P_{\text{ano}} &= 0, \\ \delta_{\text{LT}}P_{\text{sid}} &= \frac{4\pi S}{c^2 M} \left[2(\hat{\mathbf{S}} \cdot \hat{\mathbf{h}}) - (\hat{\mathbf{S}} \cdot \hat{\mathbf{m}}) \tan I \right] + \mathcal{O}(e^n), \quad n \geq 1. \end{aligned} \quad (16)$$

Here, $\hat{\mathbf{m}}$ is the unit vector directed transversely to the line of the nodes in the orbital plane, and $\hat{\mathbf{h}}$ is the unit vector of the orbital angular momentum per unit mass of the test particle (for more details, see Iorio 2016). Note that the above equations are independent of a_0 .

The effects in case of various initial conditions of the stellar orbit and the MBH spin can be explored numerically. Let us assume that, initially, $a_0 = 300$ AU or $a_0 = 800$ AU, $I_0 = \pi/4$, $\Omega_0 = 0$, and $\omega_0 = f_0 = \pi$, while e_0 varies continuously from 0.01 to 0.95. As far as the magnitude of the MBH’s angular momentum is concerned, we adopt $\chi = 1$. To avoid possible

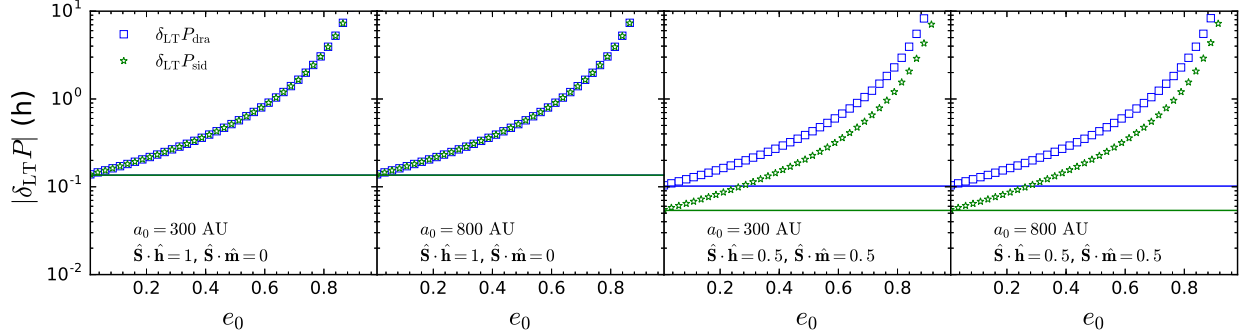


Figure 2. Perturbed orbital periods, in h, due to the 1 pN stationary Lense-Thirring gravitomagnetic field of the MBH as functions of the orbital eccentricity e_0 . The blue open square and the green star symbols show the simulation's results for the perturbed draconitic $\delta_{LT}P_{dra}$ and sidereal $\delta_{LT}P_{sid}$ periods, respectively. Different panels show the simulation's results when a_0 and the spin-orbit orientation take different values (See the legend in the bottom of each panel). The continuous blue and green lines show the values theoretically predicted by Equation 16.

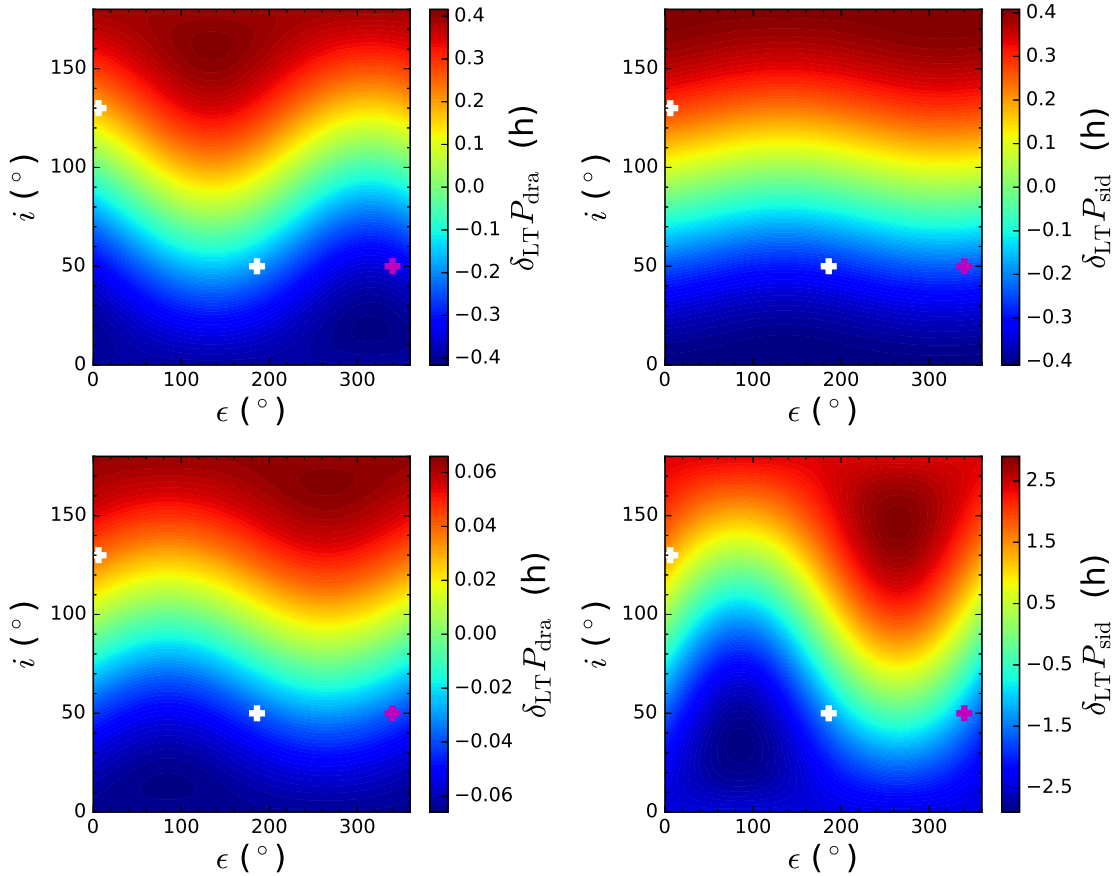


Figure 3. Upper row: draconitic and sidereal corrections for the S2 star due to the Lense-Thirring effects as functions of the i , ϵ angles characterizing the spatial orientation of the spin axis of the MBH in the GC. The white and magenta cross show the spin orientation suggested by that of the young stellar disc in the GC (Yu et al. 2016) and those from (Broderick et al. 2009), respectively. Lower row: same as in the upper row for the S0-102 star.

misunderstandings, in this section we consider the rotation of the primary to the lowest order in its angular momentum \mathbf{S} , i.e. only frame-dragging or the Lense-Thirring effect; we do not consider the quadrupole of the MBH which, according to the no-hair theorems (Geroch 1970; Hansen 1974), is of higher order in the angular momentum, being proportional to its square. The spatial orientations of the MBH's spin and of the stellar orbital plane are as such:

- The spin direction is perpendicular to the orbital plane

of the star, i.e., $\hat{\mathbf{S}} \cdot \hat{\mathbf{h}} = 1$, $\hat{\mathbf{S}} \cdot \hat{\mathbf{m}} = 0$;

- The spin direction is tilted to the orbital plane of the star, i.e., $\hat{\mathbf{S}} \cdot \hat{\mathbf{h}} = 0.5$, $\hat{\mathbf{S}} \cdot \hat{\mathbf{m}} = 0.5$.

The results are shown in Figure 2 in which $\delta_{LT}P_{dra}(e_0)$, $\delta_{LT}P_{sid}(e_0)$ are plotted as functions of e_0 for given values of some of the other orbital parameters. In the small eccentricity regime, for which a direct comparison with the analytical results provided by Equation 16 is meaningful, the agreement is

remarkable for both the spin-orbit configurations considered (left and right columns of Figure 2). For the anomalistic period, the resulting corrections are not showed as they are consistent with zero, in agreement with Equation 16. Note that the three pK effects can vary by $1 \sim 2$ orders of magnitude if we select arbitrary values of e_0 ($e_0 \lesssim 0.95$), I_0 , Ω_0 , ω_0 .

Equation 16 suggests that the gravitomagnetic corrections of the period depend strongly on the spin orientation. To explore such dependence we perform numerical simulations for the currently detected stars S2 and S0-102. Figure 3 depicts our findings for S2 and S0-102 as functions of the spatial orientation of the spin axis of the Galactic MBH. It can be noted that, the effects have both two local maximums in the $i - \epsilon$ space. For S2, $|\delta_{LT}P_{dra}|, |\delta_{LT}P_{sid}| \lesssim 0.4$ h, while for S0-102 we have $|\delta_{LT}P_{dra}| \lesssim 0.06$ h, $|\delta_{LT}P_{sid}| \lesssim 3$ h. If the spin axis is set to values given by (Broderick et al. 2009) and assuming $\chi = 0.4$, we find that $\delta_{LT}P_{dra} = -0.34$ h, and $\delta_{LT}P_{sid} = -0.23$ h for S2 and $\delta_{LT}P_{dra} = -0.04$ h, and $\delta_{LT}P_{sid} = -1.2$ h for S0-102. Alternatively, if $i = 130^\circ$, $\epsilon = 6^\circ$ (or $i = 50^\circ$, $\epsilon = 186^\circ$) and assuming $\chi = 1$, we have $\delta_{LT}P_{dra} = 0.19$ h, and $\delta_{LT}P_{sid} = 0.28$ h for S2 and $\delta_{LT}P_{dra} = 0.04$ h, and $\delta_{LT}P_{sid} = 1.3$ h for S0-102 (or $\delta_{LT}P_{dra} = -0.19$ h, and $\delta_{LT}P_{sid} = -0.28$ h for S2 and $\delta_{LT}P_{dra} = -0.04$ h, and $\delta_{LT}P_{sid} = -1.3$ h for S0-102).

3.3. The quadrupole moment effects

The theoretical quadrupole momentum effects red are given by (cfr. Equations 62-67 of Iorio (2016))

$$\begin{aligned}\delta_Q P_{dra} &= \frac{3\pi Q\mu^{3/2}}{2\sqrt{a}} \mathcal{T}_{dra}^Q + O(e^n), \quad n \geq 1, \\ \delta_Q P_{ano} &= \frac{3\pi Q\mu^{3/2}}{2\sqrt{a}} \mathcal{T}_{ano}^Q + O(e^n), \quad n \geq 1, \\ \delta_Q P_{sid} &= \frac{3\pi Q\mu^{3/2}}{2\sqrt{a}} \mathcal{T}_{sid}^Q + O(e^n), \quad n \geq 1.\end{aligned}\quad (17)$$

Here,

$$\begin{aligned}\mathcal{T}_{dra}^Q &= -4 + 6(\hat{\mathbf{S}} \cdot \hat{\mathbf{i}})^2 + 6(\hat{\mathbf{S}} \cdot \hat{\mathbf{m}})^2 \\ &+ 3\left[(\hat{\mathbf{S}} \cdot \hat{\mathbf{i}})^2 - (\hat{\mathbf{S}} \cdot \hat{\mathbf{m}})^2\right] \cos 2u_0 \\ &+ 6\left[(\hat{\mathbf{S}} \cdot \hat{\mathbf{i}})(\hat{\mathbf{S}} \cdot \hat{\mathbf{m}})\right] \sin 2u_0 \\ &- 2\left[(\hat{\mathbf{S}} \cdot \hat{\mathbf{i}})(\hat{\mathbf{S}} \cdot \hat{\mathbf{m}})\right] \cot I,\end{aligned}\quad (18)$$

$$\begin{aligned}\mathcal{T}_{ano}^Q &= -2 + 3(\hat{\mathbf{S}} \cdot \hat{\mathbf{i}})^2 + 6(\hat{\mathbf{S}} \cdot \hat{\mathbf{m}})^2 \\ &+ 3\left[(\hat{\mathbf{S}} \cdot \hat{\mathbf{i}})^2 - (\hat{\mathbf{S}} \cdot \hat{\mathbf{m}})^2\right] \cos 2u_0 + \\ &+ 6\left[(\hat{\mathbf{S}} \cdot \hat{\mathbf{i}})(\hat{\mathbf{S}} \cdot \hat{\mathbf{m}})\right] \sin 2u_0,\end{aligned}\quad (19)$$

$$\begin{aligned}\mathcal{T}_{sid}^Q &= -4 + 6(\hat{\mathbf{S}} \cdot \hat{\mathbf{i}})^2 + 6(\hat{\mathbf{S}} \cdot \hat{\mathbf{m}})^2 \\ &+ 3\left[(\hat{\mathbf{S}} \cdot \hat{\mathbf{i}})^2 - (\hat{\mathbf{S}} \cdot \hat{\mathbf{m}})^2\right] \cos 2u_0 \\ &+ 6\left[(\hat{\mathbf{S}} \cdot \hat{\mathbf{i}})(\hat{\mathbf{S}} \cdot \hat{\mathbf{m}})\right] \sin 2u_0 \\ &+ 2\left[(\hat{\mathbf{S}} \cdot \hat{\mathbf{i}})(\hat{\mathbf{S}} \cdot \hat{\mathbf{m}})\right] \tan\left(\frac{I}{2}\right).\end{aligned}\quad (20)$$

Here $\hat{\mathbf{I}}$ is the unit vector directed along the line of the nodes toward the ascending node (Iorio 2016).

The above explicit analytical expression hold only for the case $e = 0$. Similarly to Section 3.1 and 3.2, we perform several numerical simulations in order to illustrate the effects for target stars with various initial conditions. Initial conditions are $a_0 = 100$ AU or $a_0 = 300$ AU, $I_0 = \pi/4$, $\omega_0 = f_0 = \pi$, so that $u_0 = \omega_0 + f_0 = 0$; e_0 is allowed to vary continuously from 0.01 to 0.95. As far as the modeled perturbing accelerations are concerned, only the quadrupole term, proportional to S^2 in the BH case due to the no-hair theorems, is included; the Lense-Thirring one, linear in S , is switched to zero. As in Section 3.2, it is assumed $\chi = 1$. The MBH's spin and the star's orbit are oriented as follows:

- The spin direction is perpendicular to the orbital plane of the star, i.e., $\hat{\mathbf{S}} \cdot \hat{\mathbf{h}} = 1$, $\hat{\mathbf{S}} \cdot \hat{\mathbf{m}} = 0$, $\hat{\mathbf{S}} \cdot \hat{\mathbf{i}} = 0$;
- The spin direction is tilted to the orbital plane of the star, i.e., $\hat{\mathbf{S}} \cdot \hat{\mathbf{h}} = 0.5$, $\hat{\mathbf{S}} \cdot \hat{\mathbf{m}} = 0.5$, $\hat{\mathbf{S}} \cdot \hat{\mathbf{i}} = -\cos \frac{\pi}{4}$.

The results are showed in Figure 4. A comparison with the analytical predictions of Equations 17, accurate to zero order in eccentricity, with our numerical results for small values of e_0 shows a good agreement for both the spin-orbit configurations considered (left and right columns of Figure 4). For more eccentric orbits, the draconitic and the sidereal corrections keep their equality if the MBH's spin is perpendicular to the orbital plane (left column of Figure 4), while they are different for the generic spin-orbit configuration adopted in the right column of Figure 4. In both cases, the anomalistic correction does not coincide with the other two.

Similarly to Section 3.2, also in this case we explore all the quadrupole corrections of periods as functions of the spatial orientation of the spin axis of the Galactic MBH for the star S2 and S0-102. The results are showed in Figure 5. We can see that the period corrections due to the quadrupole have two local minima and two maxima in the $i - \epsilon$ plane, as it can be inferred from Equation 17 itself. For S2, the effects are within the ranges $-2 \text{ s} \lesssim \delta_Q P_{ano} \lesssim 1 \text{ s}$, $-2.5 \text{ s} \lesssim \delta_Q P_{dra} \lesssim 2.2 \text{ s}$, $-2.7 \text{ s} \lesssim \delta_Q P_{sid} \lesssim 3.3 \text{ s}$, while for S0-102 we have $-2.2 \text{ s} \lesssim \delta_Q P_{ano} \lesssim 1.1 \text{ s}$, $-15 \text{ s} \lesssim \delta_Q P_{dra} \lesssim 24 \text{ s}$, $-2.6 \text{ s} \lesssim \delta_Q P_{sid} \lesssim 2.3 \text{ s}$. Thus, the period corrections by quadrupole-induced effects are about orders of magnitude smaller than those of the Kerr-type, making the detections of them quite challenging.

4. DISCUSSION

S-stars orbiting the MBH much closer than the currently known ones are expected to be revealed by future telescopes. Their observables, i.e., the apparent proper motions and the redshifts, can be collected with high accuracy by such future facilities which can be used to reconstruct the orbital elements of the target star. Although the projected line of sight distance of the star with respect to the MBH can not be directly measured, it can be inferred by the accelerations of the proper motions and the redshift: $z = -\text{sign}(\ddot{z}) \sqrt{MG/|A| - x^2 - y^2}$, where $|A| = \sqrt{\ddot{x}^2 + \ddot{y}^2 + \ddot{z}^2}$, \ddot{x} , \ddot{y} , \ddot{z} are the accelerations in the x , y , z directions, and z represents the line of sight direction. From such measurements, it is straightforward to obtain the corresponding orbital elements and the three periods according to the measured true anomaly, argument of latitude and true longitude. If the three periods are not identical to each other, it points towards a strong evidence of the need of the general relativity corrections.

We notice that these measured periods are combinations of both the Newtonian and other GR corrections discussed in

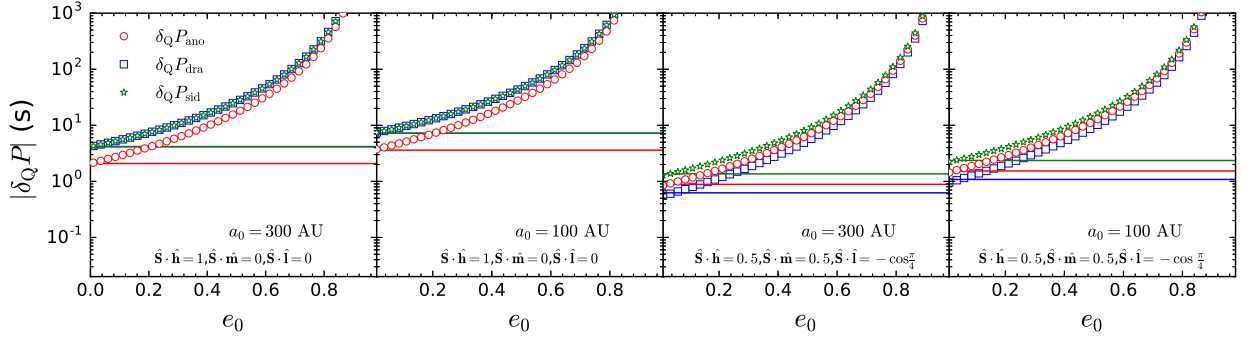


Figure 4. Perturbed orbital periods due to the MBH’s quadrupole moment (in s) which, according to the no-hair theorems, is of second order with respect to the angular momentum. The red open circle, blue square and green star symbols show the simulation’s results for the perturbed anomalous $\delta_Q P_{\text{ano}}$, draconitic $\delta_Q P_{\text{dra}}$, and sidereal $\delta_Q P_{\text{sid}}$ periods, respectively. Different panels show the simulation’s results when a_0 and the spin–orbit configuration keep different values (See the legend in the bottom of each panel). The red, blue and green continuous lines show the theoretical predictions by Equation 62–64 of Iorio (2016), valid to zero order in eccentricity.

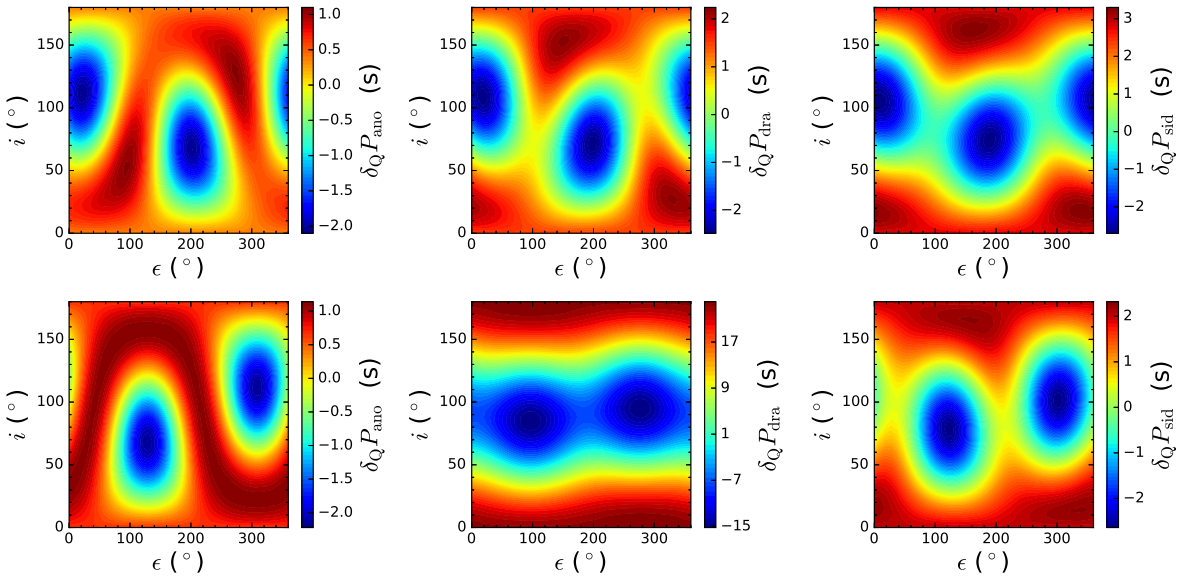


Figure 5. Upper row: anomalous, draconitic and sidereal corrections for the S2 star due to the primary’s quadrupole as functions of the i , ϵ angles characterizing the spatial orientation of the spin axis of the MBH in the Galactic center. Lower row: same as in the upper row for the S0-102 star.

Section 3. As we have showed, the period corrections due to the quadrupole momentum amount to about $1 - 10^3$ s even though the S-star can be as close as about $10 - 100$ AU from the MBH. Considering that a single exposure time of the S-stars could be comparable to or longer than such time spans, in the GC environment the quadrupole-induced period corrections may not be well constrained so to be ignorable. If the orbital elements are measured with considerable accuracy, the sum of the period corrections, given by Equation 8, 16 or the numerical simulations, can then be used to be compared with the measured three types of periods such that the spin of the MBH is determined. By such an implementation, the contributions of Kerr effects and the Schwarzschild-type effects are separated, providing independent constraints on the relativistic effects along with their orbital precession. Furthermore, the constraints could be improved if the three periods can be measured for more than a single S-star.

However, the orbital elements in Equation 8, 16 and 17 may not be clearly determined as they are defined according to the local state vectors which can not be measured directly. The practical measurement of them, and also the related period

corrections by the method mentioned above, may need to be implemented in a more complex framework. For example, the GR one which incorporates the propagation of light from the star to the observer, and also includes other complexities that are needed to accurately describe the observed motion of the star around the MBH. We defer such a realization and comprehensive studies to future works.

We also notice that the background stars can also induce Newtonian perturbations on the orbital periods (Zhang & Iorio 2017). Their most peculiar signature consists of the fact that the orbital period of the S-stars changes in every revolution (Zhang & Iorio 2017). Thus, it is expected that they should appear different with respect to those due to the general relativistic effects discussed here, which strongly suggests that these two effects are separable.

5. CONCLUSIONS

In presence of post-Keplerian accelerations, of both Newtonian and post-Newtonian origin, the degeneracy affecting the draconitic, anomalous and sidereal orbital periods of a gravitationally bound two-body system is removed. Analytical

calculations of the corresponding post-Keplerian corrections, mainly in the small eccentricity approximation, appeared recently in the literature. The extensive numerical simulations performed in the present work, applied to various orbital configurations of a target S–star orbiting the black hole which is supposed to lurk in Sgr A* at the center of the Galaxy, confirmed the previous results by extending them to highly elliptic orbits. It turned out that, for a target star with $a = 300\text{--}800$ AU and $e \approx 0.8$, the post-Newtonian Schwarzschild-type acceleration causes corrections as large as about 10 – 100 d, the Lense-Thirring ones are up to ≈ 10 h, while the quadrupole-driven ones amount to 100 s. Furthermore, we considered also the currently known S2 and S0-102 stars by numerically investigating their periods. In particular, the Schwarzschild-type anomalous corrections agreed well with the values provided by the analytical formulas in the literature; furthermore, the Lense-Thirring and quadrupole-induced orbital time intervals were studied as functions of the spatial orientation of the spin axis of the hosting black hole.

As possible directions for future work, an extension of the previously published analytical results to large values of the eccentricity would be desirable in view of a comparison with the present numerical results. Furthermore, we stress that our results have a general validity, not being restricted just to the Galactic Center; they can be straightforwardly extended also to other astronomical and astrophysical scenarios, like, e.g., exoplanets, which could turn out to be promising in view of future potential detections. Finally, the approach followed here can be extended, in principle, also to various modified models of gravity which, in the recent years, have come out to center stage. In view of their huge amount, dealing with even a fraction of them is outside the scopes of the present paper. Indeed, a comprehensive treatment of their impact on the orbital periods would deserve one or more dedicated papers, both of analytical and numerical nature. Whatever the post-Keplerian effect one is interested in, it is hoped that the present analysis may prompt dedicated studies by astronomers aimed to testing the actual measurability of the orbital periods considered here and determining the associated accuracy.

We thank the anonymous referee for her/his insightful sug-

gestions which contributed to ameliorate the manuscript. This work was supported in part by the National Natural Science Foundation of China under grant Nos. 11603083, the Fundamental Research Funds for the Central Universities grand No. 161GPY51.

REFERENCES

- Angéilil, R., Saha, P., & Merritt, D. 2010, *ApJ*, 720, 1303
 Angéilil, R., & Saha, P. 2010, *ApJ*, 711, 157
 Angéilil, R., & Saha, P. 2011, *ApJL*, 734, 19
 Broderick, A. E., Fish, V. L., Doeleman, S. S., & Loeb, A. 2009, *ApJ*, 697, 45
 Brumberg, V. A. 1991, *Essential relativistic celestial mechanics*, Bristol, England and New York, Adam Hilger, 1991, 271 p.
 Capderou M., 2005, *Satellites. Orbits and Missions*. Springer-Verlag France, Paris
 Dormand J., Prince P., 1980, *Journal of Computational and Applied Mathematics*, 6, 19
 Geroch, R. 1970, *Journal of Mathematical Physics*, 11, 2580
 Ghez, A. M., Salim, S., Weinberg, N. N., et al. 2008, *ApJ*, 689, 1044
 Gillessen S. et al., 2010, in *Proc. SPIE*, Vol. 7734, *Optical and Infrared Interferometry II*, p. 77340Y
 Gillessen, S., Eisenhauer, F., Trippe, S., et al. 2009, *ApJ*, 692, 1075
 Hairer E., Norsett S. P., Wanner G., 1987, *Springer Ser. Comput. Math.* 8
 Hansen, R. O. 1974, *Journal of Mathematical Physics*, 15, 46
 Iorio, L. 2011a, *MNRAS*, 411, 453
 Iorio, L. 2011b, *Phys. Rev. D*, 84, 124001
 Iorio, L. 2016, *MNRAS*, 460, 2445
 Kidder, L. E. 1995, *Phys. Rev. D*, 52, 821
 Kassimenko T. V., 1966, in *Trajectories of Artificial Celestial Bodies as Determined from Observations / Trajectoires des Corps Célestes Artificiels Déterminées D’après les Observations*, Kovalevsky J., ed., Springer, Berlin, pp. 1922
 Mashhoon, B., Iorio, L., & Lichtenegger, H. 2001, *Physics Letters A*, 292, 49
 Merritt, D., Alexander, T., Mikkola, S., & Will, C. M. 2010, *Phys. Rev. D*, 81, 062002
 Skidmore, W., TMT International Science Development Teams, & Science Advisory Committee, T. 2015, *Research in Astronomy and Astrophysics*, 15, 1945
 Soffel, M. H. 1989, *Relativity in Astrometry, Celestial Mechanics and Geodesy*, XIV, 208 pp. 32 figs.. Springer-Verlag Berlin Heidelberg New York. Also *Astronomy and Astrophysics Library*, 32
 Vernin J. et al., 2011, *Publ. Astron. Soc. Pac.*, 123, 1334
 Yu, Q., Zhang, F., & Lu, Y. 2016, *ApJ*, 827, 114
 Zhang, F., Lu, Y., & Yu, Q. 2015, *ApJ*, 809, 127
 Zhang, F., & Iorio, L. 2017, *ApJ*, 834, 198